

# Lamellar order, microphase structures and glassy phase in a field theoretic model for charged colloids

Marco Tarzia<sup>a</sup> and Antonio Coniglio<sup>a,b</sup>

<sup>a</sup> *Dipartimento di Scienze Fisiche and INFN sezione di Napoli, Università degli Studi di Napoli "Federico II", Complesso Universitario di Monte Sant'Angelo, via Cinthia, 80126 Napoli, Italy and*

<sup>b</sup> *Coherentia CNR-INFN*

(Dated: March 5, 2019)

In this paper we present a detailed analytical study of the phase diagram and of the structural properties of a field theoretic model with a short-range attraction and a competing long-range screened repulsion. We provide a full derivation and expanded discussion and digression on results previously reported briefly in M. Tarzia and A. Coniglio, *Phys. Rev. Lett.* **96**, 075702 (2006). The model contains the essential features of the effective interaction potential among charged colloids in polymeric solutions. We employ the self-consistent Hartree approximation and a replica approach, and we show that varying the parameters of the repulsive potential and the temperature yields a phase coexistence, a lamellar and a glassy phase. Our results suggest that the cluster phase observed in charged colloids might be the signature of an underlying equilibrium lamellar phase, hidden on experimental time scales, and emphasize that the formation of microphase structures may play a prominent role in the process of colloidal gelation.

PACS numbers: 64.60.Cn, 64.70.pf, 82.70.Dd

## I. INTRODUCTION

Colloidal suspensions are solutions of solid (or liquid) mesoscopic particles immersed into another substance [1]. These systems, like blood, proteins in water, milk, inks, or paints, are ubiquitous in our everyday life and are extremely important in biology and industry. Due to their potential applications for designing new materials with a wide range of viscoelastic properties, in the last few years there has been much interest in the role of the inter-particle potential on controlling the structural and dynamical properties of colloidal systems. By appropriately varying some control parameters (such as the composition of the solvent, the coating of the particles, the concentration of the polymers into the solvent, ...) the effective interaction potential between colloids can be suitably tuned in the experiments. It is possible to realize a hard-sphere system [2]; by adding non adsorbing polymers the hard-sphere interaction can be complemented by a short-range attraction, induced by depletion forces [3]. Recent experimental works outlined that in some cases a residual net charge on the surface of colloidal particles may be present [4, 5], thereby inducing a long-range electrostatic repulsion screened by the presence of ions in the solution. The resulting effective interaction is therefore given by a hard-core term accounting for the excluded volume, a depletion-induced narrow attractive shell and a long-range repulsive shoulder. This kind of potential is well approximated by the DLVO (after Derjaguin, Landau, Verwey and Overbeek) potential [6]. Interestingly enough, the parameters of the potential can be suitably tuned in the experiments. The depth of the attractive shell is controlled by the concentration of the polymers,  $\phi_p$ , which therefore plays the role of an inverse temperature, whereas its range is proportional to the ratio between the radius of the colloids,

$\sigma$ , and the gyration radius of the polymers,  $R_g$  (typically one has  $0.05 < R_g/\sigma < 0.2$ ). On the other hand, the addition of salt increases the number of ions in the solution responsible for the screening of the electrostatic repulsion, thereby reducing the amplitude and increasing the screening length of the Yukawa potential.

Charged colloids in polymeric solutions have recently raised a lot of interest, both from an experimental [4, 5, 7] and a theoretical [8, 9, 10, 11, 12, 13, 14] point of view. In these systems the competition between attractive and repulsive interactions on different length scales stabilizes the formation of aggregates of an optimal size and shape (*cluster phase*), characterized by a peak of the structure factor around a typical wave vector,  $k_m$ . Experimentally, such cluster phase, made up by approximately monodisperse equilibrium aggregates, can be clearly observed using confocal microscopy at low volume fraction and low temperature (high attraction strength) [4, 5, 7]. By appropriately tuning the control parameters (i.e., increasing the volume fraction or decreasing the temperature) the system progressively evolves toward a gel-like non-ergodic disordered state [5, 7] (*colloidal gelation*), where structural arrest occurs. Although intensely studied both experimentally and numerically, a theoretical understanding these phenomena is still lacking: the mechanisms inducing colloidal gelation are still unknown and many gaps remain in our present knowledge of the equilibrium phase diagram of these systems. In Ref. [8], it has been proposed that colloidal gelation is related to the formation of a Wigner glass, whose blocks are compact and thermodynamically stable clusters, with a residual long-range repulsion between them. In Ref. [10] it was instead highlighted the percolative nature of the structural arrest in charged colloids, suggesting that percolation of a spanning network of clusters with long living bonds plays a crucial role. More recently, it has been sug-

gested that the formation of partially ordered anisotropic domains and microphase structures may be responsible for physical gelation in these systems [11, 13, 14].

In a recent letter [13], we have introduced a  $\phi^4$  model with competition between a short-range attraction, described by the Ginzburg-Landau Hamiltonian, and a long-range screened repulsion, described by a Yukawa potential [15]. Albeit schematically, the model contains the essential features of the effective interaction potential among charged colloids in polymeric solutions and sheds new light on the structural properties of these systems. Here we present a detailed and extensive analytical study of this model, and a full derivation and explanation of the results previously reported briefly in [13].

We show that depending on the control parameters, there is a region of the phase diagram where usual phase separation between a colloid-rich and a colloid-poor phase takes place. Conversely, as the screening length and/or the strength of the repulsion exceeds a threshold value, phase separation is prevented. In this case, at moderately high temperature the competition between attraction and repulsion has the effect to produce microphase structures, i.e., partially ordered modulated domains which in the terminology of particle systems, correspond to the cluster phase. These modulated structures are the precursors of a first order transition to an equilibrium lamellar phase found at lower temperatures. By using a replica approach for systems without quenched disorder [16, 17], and by employing the Self-Consistent Screening Approximation (SCSA) [18, 19], we also show the presence of a glass transition line in the low temperature region, once the first order transition to the lamellar phase is avoided. The mechanism responsible for the glass transition in this case turns out to be completely different from that of molecular glass-formers: as a matter of fact, we find that glassiness is not due to the presence of a hard-core interaction, which is totally absent in our model; it is instead due to the formation of the microphase structures which order up to the size of correlation length. The geometric frustration, arising from arranging such modulated structures in a disordered fashion, leads to a complex free energy landscape and, consequently, to a dynamical slowing down.

Our results suggest that the cluster phase observed in colloidal suspensions should be followed, upon decreasing the temperature (or increasing the volume fraction), by an equilibrium periodic phase (a columnar or a lamellar phase, depending on the volume fraction). If, instead, this ordered phase is avoided, a structural arrest, corresponding to the gel phase observed in the experiments and in numerical simulations, should eventually occur. The existence of ordered phases in colloidal suspensions and the fact that the transition to the gel phase could occur in a metastable liquid, are novel predictions, which have never been considered before. Recently, the presence of such ordered phases in atomistic model systems of charged colloids interacting via the DLVO potential, has been unambiguously shown both in three [11, 14] and

in two [11, 12] dimensions.

The paper is organized as follows: in Sec. II we describe the model; in Sec. III we study the model within the self-consistent Hartree approximation; in Sec. IV we analyze the dynamics of the system in the spherical limit; in Sec. V we study the glass transition; in Sec. VI we compute the pair correlation function of the system in the real space, showing the emergence of competing length scales and emphasize the prominent role of microphase structures; in Sec. VII we summarize the results found: we discuss the resulting phase diagram and stress the connections with charged colloids. Some details of the calculations are reported in Apps. A-D.

## II. THE MODEL

We consider the standard three dimensional  $\phi^4$  field-theory with the addition of a repulsive long-range potential [13]:

$$\mathcal{H}[\phi] = \int d^3\mathbf{x} \left[ f(\phi) + \frac{1}{2} (\nabla\phi(\mathbf{x}))^2 \right] + \mathcal{H}_{LR}[\phi], \quad (1)$$

where  $\phi(\mathbf{x})$  is the scalar order parameter field, related to the concentration of colloidal particles. The local free energy has the usual Ginzburg-Landau form:

$$f(\phi) = \frac{r_0}{2} (\phi(\mathbf{x}))^2 + \frac{g}{4} (\phi(\mathbf{x}))^4. \quad (2)$$

The coefficient  $r_0$  is a temperature dependent mass proportional to the deviation  $r_0 \propto T - T_c^{MF}$  from the mean field transition temperature in absence of frustration. The long-range repulsive interaction is described by a Yukawa potential:

$$\mathcal{H}_{LR}[\phi] = \frac{W}{2} \iint d^3\mathbf{x} d^3\mathbf{x}' \frac{e^{-|\mathbf{x}-\mathbf{x}'|/\lambda}}{|\mathbf{x}-\mathbf{x}'|} \phi(\mathbf{x})\phi(\mathbf{x}'). \quad (3)$$

The local term favours the formation of a uniform condensed phase, while the long-range term energetically frustrates this condensation. In the momentum space the Hamiltonian of Eq. (1) reads:

$$\begin{aligned} \mathcal{H}[\phi] = & \frac{V}{2} \int \frac{d^3\mathbf{k}}{(2\pi)^3} \left[ r_0 + k^2 + \frac{4\pi W}{\lambda^{-2} + k^2} \right] \phi_{\mathbf{k}}\phi_{-\mathbf{k}} \\ & + \frac{gV}{4} \int \frac{d^3\mathbf{k}_1}{(2\pi)^3} \frac{d^3\mathbf{k}_2}{(2\pi)^3} \frac{d^3\mathbf{k}_3}{(2\pi)^3} \phi_{\mathbf{k}_1}\phi_{\mathbf{k}_2}\phi_{\mathbf{k}_3}\phi_{-\mathbf{k}_1-\mathbf{k}_2-\mathbf{k}_3}. \end{aligned} \quad (4)$$

The model has been also studied in [20] in the context of microemulsion. The parameters  $W$  and  $\lambda$  are, respectively, the strength and the range of the repulsive potential. For  $W = 0$  we obtain the canonical short-range ferromagnet. Interestingly, for  $\lambda \rightarrow \infty$  we recover the case of Coulomb interaction. The latter model was first introduced in Ref. [21], in the context of cuprate systems. Then, it has been further studied in many other papers (see, for instance, Refs. [22, 23, 24, 25, 26, 27])

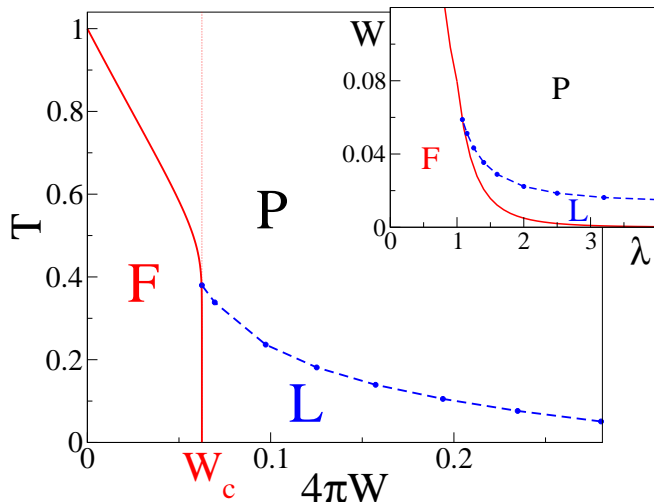


FIG. 1: (color online) **Main frame:** Phase diagram of the model obtained within the self-consistent Hartree approximation, in the frustration ( $4\pi W$ )-temperature ( $T$ ) plane, for a fixed range of the repulsive potential,  $\lambda = 2$  (and  $g = 1$ ,  $r_0 = -1$ ). The temperature is rescaled with respect to the critical temperature of the unfrustrated model,  $T_c(W = 0) = 2\pi^2/3\Lambda$ . The (red) continuous curve,  $T_c(W, \lambda)$ , corresponds to the second order phase transition from the paramagnetic to the ferromagnetic phase (with the usual Hartree critical exponents,  $\nu = 1$  and  $\gamma = 2$ ), whereas the (blue) dashed curve corresponds to the fluctuation-induced first order transition from the paramagnetic to the lamellar phase,  $T_L(W, \lambda)$ .  $W_c$  is the critical threshold of the repulsion strength, Eq. (11). **Inset:** System phase diagram in the range ( $\lambda$ )-frustration ( $W$ ) plane for a fixed temperature  $T = 0.1$ , showing the relative position of the different phases.

where it has been used to describe the phenomenology of a wide variety of systems, where competing interactions on different length scales stabilize pattern formation and the creation of spatial inhomogeneities (for a review see [28]). These systems include magnetic systems and dipolar fluids characterized by long-range Coulombic interactions [29], mixtures of block copolymers [30], water-oil-surfactant mixtures [31] and doped Mott insulator, including high  $T_c$  superconductors [32]. As a consequence, our model allows to describe and to interpret in an unified fashion the phenomenology of a broad range of different physical systems.

### III. PARAMAGNETIC, FERROMAGNETIC AND LAMELLAR PHASES WITHIN THE HARTREE APPROXIMATION

In this section we solve the model, Eq. (1), within the self-consistent Hartree approximation. This approximation amounts in replacing one factor  $\phi^2$  in the quartic term by its average  $\langle \phi^2 \rangle$ , to be determined self-

consistently [33]. For a one component order parameter there are six ways of choosing the two factor of  $\phi$  to be paired in  $\langle \phi^2 \rangle$  among the four factor of  $\phi$  in the quartic term  $g\phi^4/4$ . Hence, the self-consistent Hartree approximation consists in substituting the term  $g\phi^4/4$  with  $3g\langle \phi^2 \rangle \phi^2/2$ . With this substitution, the Hamiltonian becomes quadratic:

$$Z = \int \mathcal{D}\phi_{\mathbf{k}} e^{-\frac{\beta V}{2} \int \frac{d^3\mathbf{k}}{(2\pi)^3} \left[ r_0 + 3g\langle \phi^2 \rangle + k^2 + \frac{4\pi W}{\lambda^{-2} + k^2} \right] \phi_{\mathbf{k}} \phi_{-\mathbf{k}}}. \quad (5)$$

It is then possible to compute  $Z$  and evaluate the correlation function:

$$G(\mathbf{k}) = \langle \phi_{\mathbf{k}} \phi_{-\mathbf{k}} \rangle - \langle \phi_{\mathbf{k}} \rangle \langle \phi_{-\mathbf{k}} \rangle. \quad (6)$$

In the paramagnetic phase,  $\langle \phi_{\mathbf{k}} \rangle = 0$ , one obtains:

$$\begin{aligned} G(\mathbf{k}) &= \frac{T}{r_0 + 3g\langle \phi^2 \rangle + k^2 + \frac{4\pi W}{\lambda^{-2} + k^2}} \\ &= \frac{T}{r + k^2 + \frac{4\pi W}{\lambda^{-2} + k^2}}, \end{aligned} \quad (7)$$

where the renormalized mass term,  $r$ , has been defined as:

$$r \equiv r_0 + 3g\langle \phi^2 \rangle. \quad (8)$$

We now recall that:

$$\langle \phi^2 \rangle = G(\mathbf{x}, \mathbf{x}) = \int_{|\mathbf{k}| < \Lambda} \frac{d^3\mathbf{k}}{(2\pi)^3} G(\mathbf{k}), \quad (9)$$

where  $\Lambda$  is the ultraviolet cutoff. As a result, Eqs. (8) and (9) yield:

$$r = r_0 + 3g \int_{|\mathbf{k}| < \Lambda} \frac{d^3\mathbf{k}}{(2\pi)^3} \frac{T}{r + k^2 + \frac{4\pi W}{\lambda^{-2} + k^2}}, \quad (10)$$

which provides a self-consistent equation for the renormalized mass  $r$ . It can be shown that, apart from the factor 3, this approximation becomes exact for an  $N$ -component order parameter in the limit  $N \rightarrow \infty$  [33].

In order to solve the self-consistent equation, Eq. (10), it is convenient to define:

$$W_c \equiv \frac{1}{4\pi\lambda^4}, \quad (11)$$

and distinguish between two cases:  $W < W_c$  and  $W > W_c$ .

#### A. $W < W_c$

For  $W < W_c$  the correlation function,  $G(\mathbf{k})$ , behaves as in the standard unfrustrated case: it is a monotonically decreasing function of  $|\mathbf{k}|$ , with a maximum in  $k = 0$ , where it equals:

$$G(\mathbf{k} = \mathbf{0}) = \frac{T}{r + 4\pi W \lambda^2}. \quad (12)$$

Therefore, as  $r \rightarrow -4\pi W\lambda^2$ , the susceptibility,  $\chi = G(\mathbf{k} = \mathbf{0})/T$ , diverges. This corresponds to a usual second order phase transition towards a ferromagnetic phase. From Eq. (10), one can compute the critical temperature,  $T_c(W, \lambda)$ , given by the following relation:

$$\frac{3gT_c}{2\pi^2} \int_0^\Lambda dk \frac{1+k^2}{\left(1 + \frac{W}{W_c}\right) + k^2} = -r_0 - 4\pi W\lambda^2. \quad (13)$$

It is possible to show that the usual Hartree critical exponents are found, i.e.,  $\nu = 1$  and  $\gamma = 2$  (see App. A). In the terminology of colloidal suspensions, this means that for  $T < T_c$  the system undergoes a phase separation between a colloid-rich and a colloid-poor phase. The dependence of the critical temperature,  $T_c(W, \lambda)$ , upon  $W$  (for  $\lambda = 2$  and  $r_0 = -1$ ) is plotted in the main frame of Fig. 1 (red continuous line in Fig. 1), showing that the only effect of the repulsive interaction for  $W < W_c$  is to decrease the numerical value of  $T_c$ : for  $W = 0$  we recover the usual critical temperature of the unfrustrated system in the Hartree approximation,  $T_c(W = 0) = -\frac{2\pi^2 r_0}{3g\Lambda}$  (notice that  $r_0 < 0$ ), whereas  $T_c$  vanishes as  $W \rightarrow W_c$ .

### B. $W > W_c$

Conversely, if  $W > W_c$ , the correlation function has a maximum around a finite value of the wave vector,  $k_m$ :

$$k_m = \left(\sqrt{4\pi W} - \lambda^{-2}\right)^{1/2} = (4\pi)^{1/4} \left(\sqrt{W} - \sqrt{W_c}\right)^{1/2}. \quad (14)$$

As we shall discuss later on, the peak in the correlator indicates that the system establishes microphase structures with inverse domain size given by  $k_m$ , which characterize the incipient periodic order. Such modulated structures are the analog of the cluster phase observed in colloidal systems characterized, also in this case, by a peak in the structure factor around a characteristic wave vector corresponding to the inverse of the typical size of the clusters [5, 7, 8, 9, 10].

In  $k = k_m$ , the correlation function is given by

$$G(|\mathbf{k}| = k_m) = \frac{T}{r + 2\sqrt{4\pi W} - \lambda^{-2}}. \quad (15)$$

Therefore,  $G(|\mathbf{k}| = k_m)$  and, consequently, the fluctuations,  $\chi(|\mathbf{k}| = k_m)$ , diverge for  $r \rightarrow r_{sp} \equiv \lambda^{-2} - 2\sqrt{4\pi W}$ . As a result, also the integral of the right hand side of Eq. (10) diverges, and the self-consistent Hartree relation can be satisfied only at  $T = 0$ . This implies that for  $W > W_c$  the paramagnetic phase is stable at all finite temperatures, its spinodal line, where the susceptibility for  $|\mathbf{k}| = k_m$  diverges,  $\chi(k_m) \rightarrow \infty$ , is located at  $T = 0$ . Therefore above  $W_c$  there is no phase separation. This result is quite important for designing new materials as well as in the experimental and numerical study of colloidal systems, where it is crucial to distinguish the

slowing down due to colloidal gelation from that due to kinetic of phase separation.

Nevertheless, the system still undergoes a first order transition to a lamellar phase when the temperature is lowered below  $T_L(W, \lambda)$  (blue dashed line in Fig. 1). Such first order phase transition is induced by the fluctuations, as first discussed by Brazovskii for a related model [34] and as also found in the Coluombic case ( $\lambda \rightarrow \infty$ ) [27]. The transition temperature  $T_L(W, \lambda)$  can be determined on equating the free energy of the paramagnetic phase to that of the lamellar phase [27], as explained in App. B.

The lamellar phase is characterized by a periodic variation of the order parameter with wave-length  $l_m = 2\pi k_m^{-1}$ :

$$\langle \phi_{\mathbf{k}} \rangle = m (\delta(\mathbf{k} - \mathbf{k}_m) + \delta(\mathbf{k} + \mathbf{k}_m)), \quad (16)$$

where  $k_m$  is given in Eq. (14). Note that as  $W$  approaches  $W_c$  from above, according to Eq. (14),  $k_m$  vanishes. This signals the fact that the size of the stripes diverges on the boundary between the lamellar and the ferromagnetic phase.

Within the fluctuation approach described in App. B, it is also possible to study the stability of other kinds of ordered phases, such as columnar or periodically ordered cluster phases, which occur in numerical simulations [12, 14]. In fact, it turns out that these phases can be stable besides the lamellar phase, at lower volume fractions, i.e., for  $\langle \phi_{\mathbf{k}=\mathbf{0}} \rangle < 0$ . However, in this paper we only focus on the case  $\langle \phi_{\mathbf{k}=\mathbf{0}} \rangle = 0$ , (i.e.,  $\int d^3\mathbf{x} \langle \phi(\mathbf{x}) \rangle = 0$ ) where the only periodically ordered stable phase is the lamellar one.

### C. Phase diagram within the Hartree approximation

The results found within the self-consistent Hartree approximation are summarized in Fig. 1, where the system phase diagram in the frustration ( $4\pi W$ )-temperature ( $T$ ) plane at fixed screening length  $\lambda = 2$  (main frame) and in the screening length ( $\lambda$ )-frustration ( $W$ ) plane at fixed temperature  $T = 0.1$  (inset), is plotted, showing the relative positions of the paramagnetic (P), the ferromagnetic (F) and the lamellar (L) phases.

According to Eq. (11), by changing  $\lambda$ ,  $W_c$  changes and, hence, the phase diagram modifies. For instance, in the Coulomb limit,  $\lambda \rightarrow \infty$ , we have that  $W_c \rightarrow 0$ . As a consequence, the ferromagnetic phase reduces to the axis  $W = 0$ , for  $T < T_c(W = 0)$ . Conversely, for  $\lambda \rightarrow 0$  we have that  $W_c \rightarrow \infty$  and the lamellar phase disappears. It is interesting to observe that the dependence of the threshold  $W_c$  on the screening length  $\lambda$  is exactly the same of that found in numerical simulations of a model system for charged colloids interacting via a DLVO potential [9]: the authors find that for  $W < W_c$  the system tends to phase separate, whereas for  $W > W_c$  the preferred structures are elongated (and eventually quasi one-dimensional) finite clusters. Physically, such thresh-

old value,  $W_c$ , can be interpreted expanding the Hamiltonian, Eq. (4), up to the lowest order in  $k^2$ :

$$\begin{aligned} \mathcal{H}[\phi] \simeq & \frac{V}{2} \int \frac{d^3\mathbf{k}}{(2\pi)^3} \left[ (r_0 + 4\pi W\lambda^2) \right. \\ & \left. + (1 - 4\pi W\lambda^4) k^2 \right] \phi_{\mathbf{k}} \phi_{-\mathbf{k}} \\ & + \frac{gV}{4} \int \frac{d^3\mathbf{k}_1}{(2\pi)^3} \frac{d^3\mathbf{k}_2}{(2\pi)^3} \frac{d^3\mathbf{k}_3}{(2\pi)^3} \phi_{\mathbf{k}_1} \phi_{\mathbf{k}_2} \phi_{\mathbf{k}_3} \phi_{-\mathbf{k}_1-\mathbf{k}_2-\mathbf{k}_3}. \end{aligned} \quad (17)$$

At  $W = W_c$  the coefficient of the  $k^2$  term vanishes, implying that there is no energetic cost associated to the creation of interfaces between high density and low density regions, leading to pattern formation and to the creation of spatial inhomogeneities.

#### IV. DYNAMICS IN THE SPHERICAL LIMIT

In this section we study the dynamics of the model in the case of an  $N$ -component order parameter in the limit  $N \rightarrow \infty$ , after an instantaneous quench from high temperature. The spherical approximation is equivalent to the Hartree approximation described in the previous section (apart from the factor 3 in Eq. (10)), and allows to study analytically the dynamics. We solve the time dependent Cahn-Hilliard equation [35], following the approach taken in Refs. [36]. We obtain an exact analytical solution for the evolution of the time dependent structure factor of the system,  $G(\mathbf{k}, t)$ , and for the peak position,  $k_{max}(t)$ . In agreement with the results presented in the previous section, we find that as  $W < W_c$ , the usual spinodal decomposition occurs, and the maximum of the structure factor approaches zero as  $t^{-1/4}$  for large times. This corresponds to phase separation between a high density colloid-rich phase and low density colloid-poor one. On the other hand, for  $W > W_c$ , provided that we are on the spinodal line of the lamellar phase ( $T = 0$ ), the peak position approaches a non-zero value,  $k_m$ , given in Eq. (14), and the structure factor asymptotically approach a  $\delta$ -function peaked around  $k_m$ , signaling a lamellar order. However, since the paramagnetic phase is stable at all finite temperatures, for  $T > 0$  we find that the lamellar phase starts to form locally, but then fades away after long time and the system stays homogeneous:  $k_{max}(t)$  approaches a limiting value where the structure factor vanishes exponentially.

Let us consider the Cahn-Hilliard equation [35]:

$$\frac{\partial \phi(\mathbf{x}, t)}{\partial t} = M \nabla^2 \frac{\delta \mathcal{H}[\phi(\mathbf{x}, t)]}{\delta \phi(\mathbf{x}, t)}, \quad (18)$$

where  $M$  is related to the mobility, and  $\mathcal{H}$  is given in Eq. (1). For an  $N$ -component order parameter the above equation reads:

$$\frac{\partial \phi_\alpha(\mathbf{x}, t)}{\partial t} = M \nabla^2 \left[ \left( r + \frac{g}{N} \sum_{\beta=1}^N \phi_\beta^2(\mathbf{x}, t) - \nabla^2 \right) \phi_\alpha(\mathbf{x}, t) \right.$$

$$\left. + W \int d^3\mathbf{x}' \frac{e^{-|\mathbf{x}-\mathbf{x}'|/\lambda} \phi_\alpha(\mathbf{x}', t)}{|\mathbf{x}-\mathbf{x}'|} \right]. \quad (19)$$

In the limit  $N \rightarrow \infty$  we recover the spherical model replacing  $\frac{1}{N} \sum_{\beta=1}^N \phi_\beta^2(\mathbf{x}, t)$  by  $\langle \phi_\alpha^2(\mathbf{x}, t) \rangle$ . Here  $\langle \cdot \rangle$  represents an ensemble average over the initial configurations. By assuming the translational invariance of the pair correlation function  $G(\mathbf{x}, \mathbf{x}', t) = \langle \phi(\mathbf{x}, t) \phi(\mathbf{x}', t) \rangle = G(|\mathbf{x} - \mathbf{x}'|, t)$ , the quantity  $\langle \phi^2(\mathbf{x}, t) \rangle = G(0, t) \equiv S(t)$  becomes independent on the position  $\mathbf{x}$ . Thus, dropping the index  $\alpha$ , taking the Fourier transform over the space of Eq. (19) and multiplying both sides by  $\phi_\alpha(-\mathbf{k}, t)$  we obtain the equation of motion for the time dependent structure factor,  $G(\mathbf{k}, t) = \langle \phi_\alpha(\mathbf{k}, t) \phi_\alpha(-\mathbf{k}, t) \rangle$ :

$$\frac{\partial G(\mathbf{k}, t)}{\partial t} = -Mk^2 \left[ r + gS(t) + k^2 + \frac{4\pi W}{\lambda^{-2} + k^2} \right] G(\mathbf{k}, t). \quad (20)$$

By replacing  $\frac{1}{N} \sum_{\beta=1}^N \phi_\beta^2(\mathbf{x}, t)$  by  $S(t)$  we have, in fact, enabled a linearization of Eq. (19), ‘‘preaveraging’’ the nonlinear term. Now Eq. (20) can be readily integrated to obtain:

$$G(\mathbf{k}, t) = G(\mathbf{k}, 0) e^{-Mk^2 \left[ Q(t) + k^2 t + \frac{4\pi W t}{\lambda^{-2} + k^2} \right]}, \quad (21)$$

where  $Q(t)$  is defined by

$$Q(t) = \int_0^t dt' [gS(t') + r]. \quad (22)$$

To complete the solution,  $S(t)$  must be computed self-consistently. As shown in App. C, one can obtain an expression for the time dependent structure factor, Eq. (C7), and an equation for the evolution of the peak position:

$$\begin{aligned} \exp \left[ Mt \left( 1 - \frac{4\pi W}{(\lambda^{-2} + k_{max}^2(t))^2} \right) k_{max}^4(t) \right] \\ = P \times \left[ 1 - \frac{4\pi W \lambda^{-2}}{(\lambda^{-2} + k_{max}^2(t))^3} \right]^{1/2} \frac{\sqrt{Mt}}{k_{max}(t)}, \end{aligned} \quad (23)$$

where the function  $P$  is given in Eq. (C5). Taking the logarithm of both sides of Eq. (23) and dividing by  $Mt$  we obtain an asymptotic expression for  $k_{max}(t)$ , Eq. (C8), which is readily analyzed in the limit  $t \rightarrow \infty$ . Careful analysis show that depending on the values of  $W$  and  $\lambda$ , different solutions of this equation are found. In particular, one needs again to distinguish between the cases  $W < W_c$  and  $W > W_c$ .

##### A. $W < W_c$

For  $W < W_c$  the solution of Eqs. (23) and (C8) is given by:

$$k_\infty \equiv \lim_{t \rightarrow \infty} k_{max}(t) = 0, \quad (24)$$

corresponding to the usual spinodal decomposition. Using Eq. (C8) we find that the usual  $N \rightarrow \infty$  domain growth exponent of the canonical short-range ferromagnet with conserved order parameter is found:

$$k_{max}(t) \sim t^{-1/4}. \quad (25)$$

Obviously, this solution can be obtained provided that we are below the critical point,  $r < -4\pi W \lambda_0^2$  [ $T < T_c(W)$ ], otherwise no spinodal decomposition takes place and the system remains in the paramagnetic phase.

### B. $W > W_c$

For  $W > W_c$  the solution of Eqs. (23) and (C8) is given by:

$$k_\infty^2 = \sqrt{4\pi W} - \lambda^{-2} = k_m^2, \quad (26)$$

where the wave vector  $k_\infty$  coincides with that defined in Eq. (14). In this case, the peak position reaches a nonzero steady state value for large times and the structure factor asymptotically approaches a  $\delta$ -function peaked around a finite value of the wave vector  $k_m$ . This situation corresponds to the lamellar phase and  $k_m$  is the inverse domain size. In particular, for earlier times (such that  $4\pi W \ll k_{max}^4(t)$ ), using Eq. (C8), we have that:

$$k_{max}(t) \sim \left(\frac{3}{4} \ln t\right)^{1/4} t^{-1/4}. \quad (27)$$

Thus, apart from the logarithmic factor, in this regime  $k_{max}(t)$  behaves as the standard solution of the unfrustrated short-range ferromagnet in the large  $N$  limit in the case of usual spinodal decomposition. However, at later times,  $k_{max}(t)$  saturates at  $k_m$  as a power law:

$$k_{max}^2(t) \sim k_m^2 + C t^{-1/2}. \quad (28)$$

According to Eq. (C7), the structure factor  $G(\mathbf{k}, t)$  can be approximated by a Gaussian centred about  $k_m$  and with width

$$\Delta k \sim \frac{(4\pi W)^{1/4}}{\left[\sqrt{4Mt}(\sqrt{4\pi W} - \lambda^{-2})\right]}, \quad (29)$$

which in the limit  $t \rightarrow \infty$  approaches a  $\delta$ -function centred in  $k_m$ , as stated before.

However, this situation can occur only provided that we are on the spinodal line of the lamellar phase, located at  $T = 0$ . As discussed in the previous section, the expression of the spinodal line reads (both in the Hartree approximation and in the large  $N$  limit):

$$r_{sp}(W, \lambda) = -2\sqrt{4\pi W} + \lambda^{-2}. \quad (30)$$

Indeed, as  $r > r_{sp}(W, \lambda)$  (i.e.,  $T > 0$ ), from Eq. (C8) we have that  $k_{max}(t)$  approaches exponentially a limiting value,  $k_\infty^2 = -(r + \lambda^{-2})/2$ :

$$k_{max}^2(t) = k_\infty^2 + C \times \frac{e^{-M(W - W_{sp})t}}{\sqrt{Mt}}, \quad (31)$$

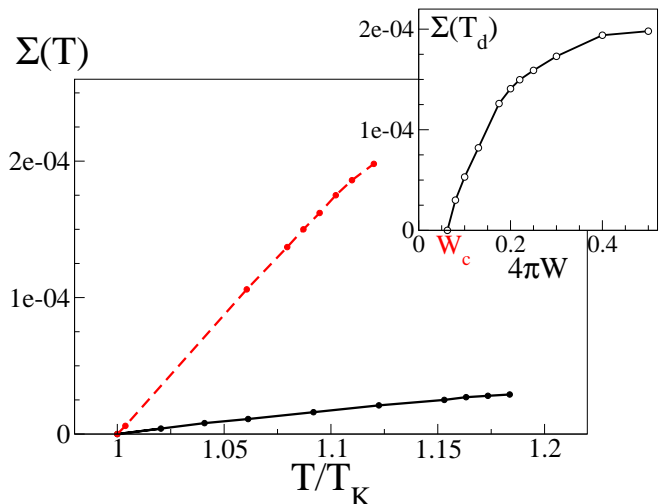


FIG. 2: (color online) **Main frame:** Complexity,  $\Sigma$ , as a function of  $T/T_K$  for  $4\pi W = 0.5$  (red dashed curve) and  $4\pi W = 0.08$  (black continuous curve), for a fixed value of the range of the repulsive potential,  $\lambda = 2$ , and for  $g = 1$  and  $r_0 = -1$ . At high temperature ( $T > T_d$ ) the system is in the paramagnetic phase and the complexity is zero. At  $T = T_d$  the complexity discontinuously jumps to a finite value, signaling the emergence of a complex free energy landscape. The complexity decreases as the temperature is decreased and vanishes at  $T_K$  where the thermodynamic transition to a 1RSB glassy phase takes place. **Inset:** Complexity at the dynamical transition temperature,  $\Sigma(T_d)$ , plotted as a function of the strength of the repulsive potential,  $4\pi W$ . As  $W$  decreases,  $\Sigma(T_d)$  decreases. At  $W = W_c$ , the glassy phase disappears.

where  $W_{sp} = (\lambda^{-2} - r)^2 / 16\pi$ . Consequently,  $P$ , Eq. (C5), asymptotically vanishes in an exponential fashion, signaling that the periodic pattern fades. At the spinodal line we have that  $W = W_{sp}$ , which gives back Eq. (28).

In conclusion, the analysis of the dynamics in the spherical limit indicates that for  $W < W_c$  the system undergoes a phase separation between a colloid-rich phase and a colloid-poor one. On the other hand, for  $W > W_c$  and  $T > 0$  the system starts to form microphase structures and periodically ordered modulated domains, as signaled by a peak in the structure factor which grows in time and whose position seems to approach  $k_m$ . However, since the paramagnetic phase is stable at all finite temperatures, the microphase structures have a finite lifetime. The lamellar order is fully established only at  $T = 0$ .

## V. THE GLASS TRANSITION

Since the paramagnetic phase is stable at all finite temperatures, the first order transition to the lamellar phase can be kinetically avoided. It is then possible to supercool the system in the (meta-stable) homogeneous phase

below the first order transition line,  $T_L(W, \lambda)$ , as much as one can obtain supercooled liquids by performing fast enough coolings below the melting temperature avoiding crystallization. Experimental [37] and numerical [38, 39] results show that, indeed, these systems exhibit long-time relaxations similar to that observed in glasses. Recent results have clearly shown the presence of a glass transition in the Coulomb case ( $\lambda \rightarrow \infty$ ) [25, 26, 27, 40].

### A. General formalism

In order to study the glass transition in our model, we use a replica approach introduced in Ref. [16] and then developed in Ref. [17], formulated to deal with system without quenched disorder, which allows to compute the complexity,  $\Sigma$ .

Our aim is to derive the free energy landscape of the model. The equilibrium free energy, defined as  $F = -T \ln Z$ , is relevant only if the system is able to explore the entire phase space. This is not the case in the glassy phase, where the system is frozen in metastable states. In order to scan the locally stable field configurations, we introduce an appropriate symmetry breaking field  $\psi(\mathbf{x})$ , and compute the following partition function [16]:

$$\tilde{Z}[\psi] = \int \mathcal{D}\phi \exp\left(-\beta\mathcal{H}[\phi] - \frac{u}{2} \int d^3\mathbf{x} [\psi(\mathbf{x}) - \phi(\mathbf{x})]^2\right), \quad (32)$$

where  $u$  denotes the strength of the coupling. Since  $u > 0$ , the introduction of the pinning field  $\psi(\mathbf{x})$  forces the order parameter  $\phi(\mathbf{x})$  to assume configurations close to  $\psi(\mathbf{x})$ . Therefore, the free energy

$$\tilde{f}[\psi] = -T \ln \tilde{Z}[\psi] \quad (33)$$

will be low if  $\psi(\mathbf{x})$  equals to configurations which locally minimize  $\mathcal{H}[\phi]$ . Thus, in order to scan all metastable states, we have to sample all configurations of the field  $\psi$ , weighted with  $\exp(-\beta\tilde{f}[\psi])$ :

$$\tilde{F} = \lim_{u \rightarrow 0^+} \frac{\int \mathcal{D}\psi \tilde{f}[\psi] \exp(-\beta\tilde{f}[\psi])}{\int \mathcal{D}\psi \exp(-\beta\tilde{f}[\psi])}. \quad (34)$$

Therefore,  $\tilde{F}$  is a weighted average of the free energy in the various metastable states. If there are only a few local minima (i.e., a non-extensive number of local minima) of free energy  $\tilde{f}$  equal to  $F$ , we have that  $\tilde{F}$  equals the true free energy  $F$  of the system. However, in case of the emergence of an exponentially large number of metastable states with large barriers between them, a nontrivial contribution arises from the above integral even in the limit  $u \rightarrow 0^+$  and  $\tilde{F}$  differs from  $F$ . This allows to identify the configurational entropy  $\Sigma$  [16, 17]:

$$F = \tilde{F} - T\Sigma. \quad (35)$$

In order to get an explicit expression for  $\Sigma$  we introduce replicas. The replicated free energy reads:

$$F(m) = - \lim_{u \rightarrow 0^+} \frac{T}{m} \ln \int \mathcal{D}\psi \left(\tilde{Z}[\psi]\right)^m, \quad (36)$$

from which, evidently,  $\tilde{F}$  can be obtained as

$$\tilde{F} = \left. \frac{\partial m F(m)}{\partial m} \right|_{m=1}, \quad (37)$$

and hence, according to Eq. (35)

$$\Sigma = \left. \frac{1}{T} \frac{\partial F(m)}{\partial m} \right|_{m=1}. \quad (38)$$

Using Eq. (32) and integrating over  $\psi$ , we get:

$$Z(m) = \lim_{u \rightarrow 0^+} \int \prod_{a=1}^m \mathcal{D}\phi^a \exp\left(-\beta \sum_{a=1}^m \mathcal{H}[\phi^a] + \frac{u}{2m} \sum_{a,b=1}^m \int d^3\mathbf{x} \phi^a(\mathbf{x}) \phi^b(\mathbf{x})\right). \quad (39)$$

The partition function of Eq. (39) is formally equivalent to that of a system in a quenched random field analyzed by means of the replica trick, such as the random field Ising model (RFIM). The only difference is that in this case the limit  $m \rightarrow 1$  must be taken. We can thus use the techniques developed to deal with such systems [19]. The matrix correlation function of the problem of Eq. (39) obeys the following Dyson equation:

$$G_{ab}^{-1}(\mathbf{k}) = G_0^{-1}(\mathbf{k})\delta_{ab} + \Sigma_{ab}(\mathbf{k}) - \frac{u}{m}, \quad (40)$$

where  $G_0^{-1}(\mathbf{k})$  is the propagator of the free unreplicated theory, Eq. (7), and  $\Sigma_{ab}(\mathbf{k})$  is the self-energy in the replica space. If we find that, due to the ergodicity-breaking coupling constant  $u$ ,  $\Sigma_{ab}(\mathbf{k})$  has finite off-diagonals elements, we can conclude that there must be an energy landscape sensitive to that infinitesimal perturbation, leading to a glassy dynamics. On the other hand, if the self-energy is diagonal, the dynamics is ergodic and the system is in the liquid phase.

### B. The Self-Consistent Screening Approximation

In the following we use the self-consistent screening approximation (SCSA) [18, 19, 25, 26], which consists in introducing a  $N$ -component version of the model with  $\phi = (\phi_1, \dots, \phi_N)$  and coupling constant  $g/N$  and summing self-consistently all the diagrams of order  $1/N$  (see Fig. 7). This approximation is exact up to order  $1/N$ . At the end of calculations we will consider the scalar case,  $N = 1$  [41]. Since the attractive coupling between replicas is symmetric with respect to the replica index, we



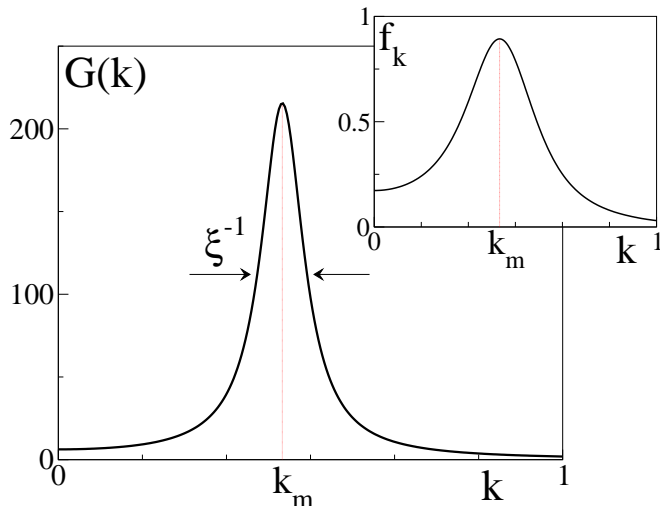


FIG. 3: **Main frame:** Momentum dependence of the correlation function,  $G(\mathbf{k})$ , for  $4\pi W = 0.2$  and  $\lambda = 2$  at  $T = T_d$ , showing that it is peaked around the typical modulation wave vector  $k_m$  with width  $\xi^{-1}$ , given by the inverse of the correlation length, signaling the fact that microphase structures establish over a finite range  $\xi$ . **Inset:** Momentum dependence of the non ergodicity parameter,  $f_{\mathbf{k}}$ , for the same values of  $W$ ,  $\lambda$  and  $T$ .

assume the following structure of the matrix correlation function:

$$G_{ab}(\mathbf{k}) = [\mathcal{G}(\mathbf{k}) - \mathcal{F}(\mathbf{k})] \delta_{ab} + \mathcal{F}(\mathbf{k}), \quad (41)$$

i.e., with diagonal elements  $\mathcal{G}(\mathbf{k})$  and off-diagonal elements  $\mathcal{F}(\mathbf{k})$ . It can be shown that for system with quenched disorder (such as the RFIM), this ansatz turns out to be equivalent to the one-step replica symmetry breaking ansatz (1RSB). While the diagonal correlator can be interpreted as the usual (one time) correlation function, i.e.,

$$T\mathcal{G}(\mathbf{k}) = \langle \phi_{\mathbf{k}} \phi_{-\mathbf{k}} \rangle, \quad (42)$$

the off-diagonal term can be interpreted as measuring the long-time correlations:

$$T\mathcal{F}(\mathbf{k}) = \lim_{t \rightarrow \infty} \langle \phi_{\mathbf{k}}(t) \phi_{-\mathbf{k}}(0) \rangle. \quad (43)$$

Hence,  $\mathcal{F}(\mathbf{k})$  vanishes in the paramagnetic phase while is finite in the glassy one.

As shown in Ref. [26] and in App. D, within the SCSA the expressions of the correlators can be found by solving numerically a set of coupled integral equations, Eqs. (D8)-(D16). After that, according to Eqs. (D19) and (D20) we are able to compute the complexity,  $\Sigma$ .

### C. Results

We have fixed the range of the repulsive potential to  $\lambda = 2$  and we have studied the behaviour of the complex-

ity for different values of the strength of the repulsion,  $W$ , and of the temperature  $T$ . The model undergoes a glass transition of the same nature of that found in discontinuous spin glasses [13, 25, 26]. In Fig. 2 the behaviour of the configurational entropy is plotted for two different values of  $W$  as a function of the temperature. For a given value of the strength of the repulsion  $W$ , at high temperature,  $\mathcal{F}(\mathbf{k})$  vanishes, leading to a vanishing complexity, corresponding to the fact that the system is in the liquid phase. At  $T = T_d(W)$  the configurational entropy jumps discontinuously to a finite value, signaling the emergence of an exponentially large number of metastable states. At this temperature a glassy dynamics sets in, corresponding to a non-zero value of the long time correlation function  $\mathcal{F}(\mathbf{k})$ . The complexity decreases as the temperature is decreased and vanishes at  $T_K(W)$ . At this temperature, called the Kauzmann temperature, an ideal thermodynamic glass transition to a 1RSB glassy phase takes place. Note that, in agreement with the results presented in the previous section, the glass transition disappears for  $N \rightarrow \infty$ , when the corrections due to the diagrams of order  $1/N$  are not taken into account.

In order to characterize the nature of the glass transition, we examine the properties of the correlation functions [13]. In the main frame of Fig. 3 the diagonal part of the correlator,  $\mathcal{G}(\mathbf{k})$ , is plotted as a function of the wave vector at the dynamical transition temperature  $T_d$ , showing that the correlation function is clearly peaked around a maximum located in  $k_m$ , whose value is given in Eq. (14). As shown in the next section, the width of such maximum,  $\xi^{-1}$ , allows to identify the inverse of the correlation length. The shape of  $\mathcal{G}(\mathbf{k})$  indicates that, although no periodic order occurs ( $\langle \phi_{\mathbf{k}_m} \rangle = 0$ ), a lamellar structure of wave length  $l_m = 2\pi k_m^{-1}$  over a finite range  $\xi$  is formed. These microphase structures are the analog of the cluster phase observed in colloidal systems. The system forms a mosaic of such modulated structures, periodically ordered over length scales smaller than the correlation length  $\xi$ , and randomly assembled in a disordered fashion over larger length scales. The defects and the imperfections in the perfect stripe arrangements give rise to the tails in the correlation function. The lower is the temperature, the more pronounced is the peak of  $\mathcal{G}(\mathbf{k})$  around the maximum in  $k_m$ , signaling the fact that  $\xi$  increases as the temperature is decreased. At  $T = T_d$ , where  $\xi \gtrsim 2l_m$ , these microphase structures establish over a length larger than their modulation length and becomes frozen. The glass transition arises from the fact that there are many possible configurations to arrange such modulated structures in a disordered fashion, leading to the emergence of metastable states.

The characteristic wave length,  $k_m^{-1}$ , dominates also the dynamics as indicated by the momentum dependence of the non ergodicity parameter

$$f_{\mathbf{k}} \equiv \lim_{t \rightarrow \infty} \frac{\langle \phi_{\mathbf{k}}(t) \phi_{-\mathbf{k}}(0) \rangle}{\langle \phi_{\mathbf{k}}(t) \phi_{-\mathbf{k}}(t) \rangle} = \frac{\mathcal{F}(\mathbf{k})}{\mathcal{G}(\mathbf{k})}, \quad (44)$$



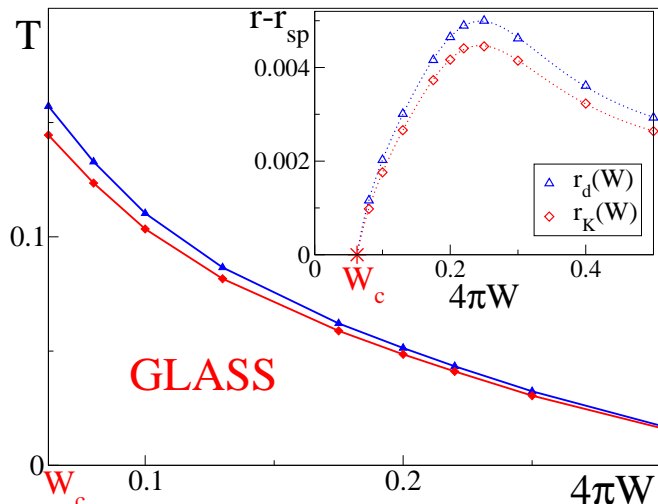


FIG. 4: (color online) **Main frame:** Dynamical (blue curve and triangles) and thermodynamical (red curve and diamonds) transition temperature to the glassy phase, as a function of the strength of the repulsive potential,  $4\pi W$ , for  $\lambda = 2$ . **Inset:** Values of the renormalized mass,  $r_d$  and  $r_K$ , corresponding, respectively, to the dynamical and the thermodynamical glass transition temperatures, as a function of  $4\pi W$ . In the figure the difference between  $r_d(W)$  (red curve and triangles) and  $r_K(W)$  (blue curve and diamonds) and the minimum value of the renormalized mass,  $r_{sp}(W)$ , is plotted. The figure shows that as  $W \rightarrow W_c$ , both  $r_d$  and  $r_K$  approach  $r_{sp}(W)$ , signaling that  $T_{d,K}(W_c) = 0$ .

plotted in the inset of Fig. 3 at  $T = T_d$ . Basically,  $f_{\mathbf{k}}$  represents the height of the plateau reached by the correlation function of the density fluctuations of wave vector  $\mathbf{k}$  after infinite time. From Eq. (44) one immediately observes that as  $\mathcal{F}(\mathbf{k}) = 0$  ( $T > T_d$ ), also the non ergodicity parameter,  $f_{\mathbf{k}}$ , vanishes: the system is in an ergodic phase, since all the correlation functions relax to zero. On the other hand, at  $T = T_d$  the ergodicity is broken. The presence of a maximum of  $f_{\mathbf{k}}$  located in  $|\mathbf{k}| = k_m$  signals the fact that structural arrest is more pronounced over length scales of order  $l_m$ . The width of the maximum of the non ergodicity parameter,  $\Upsilon^{-1}$ , can be tied to the emergence of a new length scales. Indeed, the height of the plateau decays as  $||\mathbf{k}| - k_m| > \Upsilon^{-1}$ , and  $\Upsilon$  represents the typical length scale over which defects and imperfections in the periodically modulated pattern are allowed to wander and to diffuse over long times [25, 26].

In Fig. 4 the dynamical transition temperature  $T_d(W)$  and the ideal one  $T_K(W)$  are plotted as a function of the frustration  $4\pi W$ , for a fixed value of the range of the repulsive potential,  $\lambda = 2$ . It is also interesting to study the behaviour of  $r_d(W)$  and  $r_K(W)$ , i.e., the values of the renormalized mass  $r$  corresponding, respectively, to the dynamical and to the thermodynamical transition temperature. More precisely, in the inset of Fig. 4,  $r_d(W) - r_{sp}(W)$  and  $r_K(W) - r_{sp}(W)$  are plotted, where

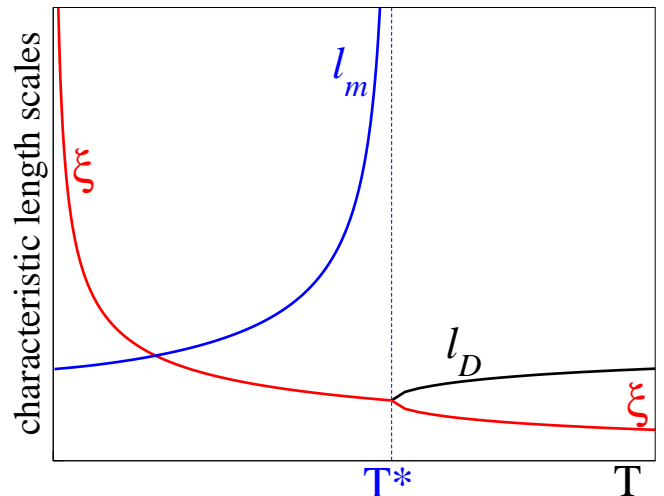


FIG. 5: (color online) Temperature dependence of the characteristic length scales. At high temperatures,  $T > T^*$ , the system behaves as a fluid of charges of linear size  $\xi$  (red curve) and screening length  $l_D$  (black curve). At  $T^*$  this description breaks down and the competition between attraction and repulsion produces microphase structures with interstripe distance  $l_m$  (blue curve), established over a finite range  $\xi$ . The modulation length,  $l_m$ , decreases as the temperature is decreased and at low temperature equals  $2\pi k_m^{-1}$ . Conversely, the correlation length,  $\xi$ , increases as the temperature is decreased and diverges at  $T \rightarrow 0$  at the spinodal line of the homogeneous phase. Glassiness emerges when  $\xi \gtrsim 2l_m$ . On the contrary, the modulated structures progressively fade as  $\xi \lesssim l_m$ .

$r_{sp}(W)$  is the minimum value of the renormalized mass (corresponding to  $T = 0$ ), whose expression is given in Eq. (30). The figure clearly shows that the glassy phase disappears as  $W \rightarrow W_c$ , where we find that  $r_{d,K}(W_c) \rightarrow r_{sp}(W_c)$ , i.e.,  $T_d(W_c) = T_K(W_c) = 0$ . (Nevertheless, we have that  $\lim_{W \rightarrow W_c^+} T_{d,K}(W) \neq T_{d,K}(W_c) = 0$ ). These results can be interpreted if one observes that, according to Eq. (14), the size of the modulated structures increases as  $W$  is decreased and diverges as  $W \rightarrow W_c$ . In fact, for purely geometrical reasons, the larger is the modulation length, the smaller is the number of metastable configurations to arrange the microphase structures in a disordered fashion. As a consequence, the number of metastable states (i.e., the complexity) vanishes as  $W \rightarrow W_c$  and the glassy phase disappears. This is clearly outlined by the inset of Fig. 2, which shows that the complexity computed at the dynamical transition temperature tends to zero as  $W \rightarrow W_c$ .

## VI. MODULATED STRUCTURES AND CHARACTERISTIC LENGTH SCALES

In this section we analyze more accurately the nature of the microphase structures which are formed due to the competition between attraction and repulsion on different length scales. This investigation provides many insights on the nature of the cluster phase observed in colloidal suspensions and on the physical mechanisms inducing the structural arrest in these systems.

Let us consider the case  $W > W_c$ , where the correlation function,  $G(\mathbf{k})$ , is peaked around the typical modulation wave vector,  $k_m$ . In the following we compute the correlation function in real space (within the self-consistent Hartree approximation, or, equivalently, in the spherical limit) and we show that different length scales emerge in the system [23, 42]. The pair correlator in real space is determined by computing the Fourier transform of  $G(\mathbf{k})$ , given in Eq. (7):

$$\begin{aligned} G(\mathbf{x}) &= \frac{1}{(2\pi)^3} \int d^3\mathbf{k} G(\mathbf{k}) e^{i\mathbf{k}\cdot\mathbf{x}} \\ &= \frac{T}{2\pi^2|\mathbf{x}|} \int dk \frac{k(\lambda^{-2} + k^2) \sin(kx)}{(k^2 + \zeta^2)(k^2 + \kappa^2)}, \end{aligned} \quad (45)$$

where

$$\zeta^2, \kappa^2 = \frac{(r + \lambda^{-2}) \pm \sqrt{(r - \lambda^{-2})^2 - 16\pi W}}{2}. \quad (46)$$

The above equation marks a crossover temperature  $T^*$ , corresponding to the temperature at which the renormalized mass equals:

$$r^* = \lambda^{-2} + 2\sqrt{4\pi W}. \quad (47)$$

### A. High temperature: $r > r^*$

For high enough temperatures,  $r > r^*$  (i.e.,  $T > T^*$ ), the argument of the square root of the right hand side of Eq. (46) is positive. Consequently,  $\zeta^2$  and  $\kappa^2$  assume real values and the integral, Eq. (45), can be easily evaluated by applying the residue theorem to the poles lying on the imaginary axis at  $k = \pm i\zeta, \pm i\kappa$ , leading to

$$G(\mathbf{x}) = \frac{T [(\zeta^2 - \lambda^{-2}) e^{-\zeta|\mathbf{x}|} + (\lambda^{-2} - \kappa^2) e^{-\kappa|\mathbf{x}|}]}{4\pi|\mathbf{x}|(\zeta^2 - \kappa^2)}. \quad (48)$$

The above expression clearly indicates the emergence of two characteristic length scales,  $\xi = |\Re\{\zeta\}|^{-1}$  and  $l_D = |\Re\{\kappa\}|^{-1}$ . The former plays the role of the correlation length of the canonical short-range ferromagnet and at high temperature behaves as:

$$\xi \sim r^{-1/2}. \quad (49)$$

The other length  $l_D$ , instead, is a renormalized screening length, and for high temperature tends to

$$l_D \sim \lambda, \quad (50)$$

the range of the repulsive potential. Therefore, the system at high temperatures,  $T > T^*$ , behaves as a fluid of charges of linear size  $\xi$  and screening length  $l_D$ . The temperature dependence of  $\xi$  and  $l_D$  is shown in Fig. 5.

### B. Low temperature: $r < r^*$

Conversely, for  $r < r^*$  (i.e.,  $T < T^*$ ) the argument of the square root of Eq. (46) becomes negative. Consequently,  $\zeta^2$  and  $\kappa^2$  assume complex values. The analytic continuation of Eq. (48) to the low temperature region reads:

$$\begin{aligned} G(\mathbf{x}) &= \frac{T}{16\pi|\mathbf{x}|\kappa_1\kappa_2} e^{-\kappa_1|\mathbf{x}|} \left[ (2\kappa_1\kappa_2 - \lambda^{-2}) \cos(\kappa_2|\mathbf{x}|) \right. \\ &\quad \left. + (\kappa_2^2 - \kappa_1^2 - \lambda^{-2}) \sin(\kappa_2|\mathbf{x}|) \right], \end{aligned} \quad (51)$$

where  $\kappa = \kappa_1 + i\kappa_2$ . This expression implies that, although no periodic order occurs ( $\langle\phi_{\mathbf{k}_m}\rangle = 0$ ), a lamellar structure of wave length  $l_m$  over a finite range  $\xi$  is formed. The modulation length is given by:

$$l_m = 2\pi|\kappa_2|^{-1} = 4\pi \left[ 2\sqrt{r\lambda^{-2} + 4\pi W} - r - \lambda^{-2} \right]^{-1/2}, \quad (52)$$

whereas, according to Eq. (51), the correlation length reads:

$$\xi = |\kappa_1|^{-1} = 2 \left[ (r + \lambda^{-2}) + 2\sqrt{r\lambda^{-2} + 4\pi W} \right]^{-1/2}, \quad (53)$$

and gives the range over which the microphase structures are formed. The temperature dependence of the characteristic length scales present in the system is shown in Fig. 5. The correlation length increases as the temperature is decreased and diverges as  $T$  goes to zero, where the spinodal line of the paramagnetic phase is located. At low temperatures we have  $l_m = 2\pi k_m^{-1}$ , where  $k_m$  is the characteristic wave vector defined in Eq. (14). Conversely, as  $T \rightarrow T^{*-}$ , the modulation length  $l_m$  diverges as  $(r^* - r)^{-1/2}$ . Interestingly enough, it turns out that the glass transition emerges at temperatures at which  $\xi \geq 2l_m$ , as conjectured in Ref. [26]: the microphase structures form over a length larger than their modulation length and become frozen. The glass transition arises from the fact that there are many possible configurations to arrange such modulated structures in a disordered fashion, leading to a great number of metastable states. As the temperature is increased, the cluster phase continuously fades approximately at the temperature at which  $\xi \lesssim l_m$ : the microphase structures are ordered over a length scale smaller than their own modulation length and the system becomes homogeneous. Such a crossover temperature at which approximately the modulated structures fades and the system is homogeneous corresponds to the black dotted line of Fig. 6.

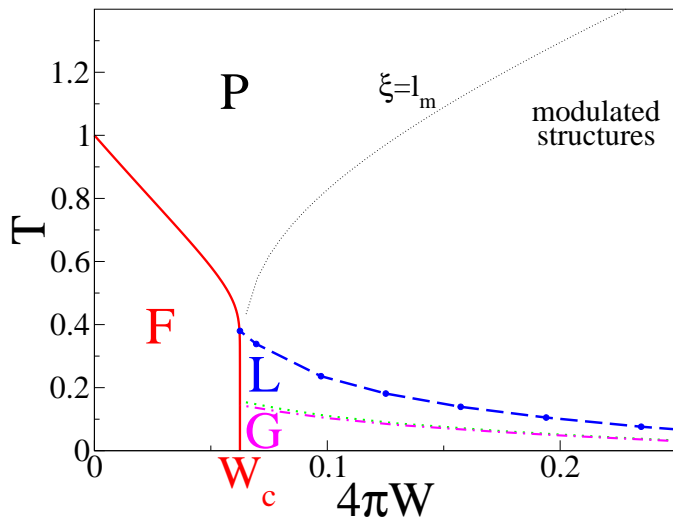


FIG. 6: System phase diagram in the frustration ( $4\pi W$ )-temperature ( $T$ ) plane, for a fixed value of the screening length of the repulsive potential,  $\lambda = 2$ , and for  $g = 1$  and  $r_0 = -1$ . The temperature is scaled with respect to the critical temperature of the unfrustrated system,  $T_c(W = 0) = -2\pi^2 r_0 / 3g\Lambda$ . For  $W < W_c$  a second order phase transition with the usual Hartree critical exponents from a paramagnetic phase (P) to a ferromagnetic (F) one is found, by lowering the temperature below  $T_c(W, \lambda)$  (red continuous curve). In the terminology of colloidal system this corresponds to a phase separation between a colloid rich and a colloid poor phase. For  $W > W_c$  the phase separation is prevented and, instead, a first order transition to a lamellar phase (L), characterized by a periodic variation of the density, is found at  $T_L(W, \lambda)$  (blue dashed line). Such a first order transition can be avoided and, in this case, at lower temperature a transition to a glassy phase (G) is found, characterized by a dynamical,  $T_d(W, \lambda)$  (green dotted curve), and by a thermodynamical,  $T_K(W, \lambda)$  (magenta dashed-dotted curve) transition. The black dotted line represent a crossover temperature, corresponding to the temperature at which the correlation and the modulation lengths equal,  $\xi \simeq l_m$ , and the system establishes microphase structures, which are the analog of the clusters observed in colloidal systems.

## VII. PHASE DIAGRAM AND CONCLUDING REMARKS

The results found in the previous sections are summarized in Fig. 6, where the complete phase diagram of the system is presented, showing the relative position of the different phases. The model, albeit schematically, retains the essential physics of charged colloids in polymeric solutions, where the competition between attraction and repulsion on different length scales plays a prominent role. The results found provide many insights on the equilibrium phase diagram of colloidal suspensions, as well as on the physical mechanisms responsible for the formation of modulated structures and for the structural arrest.

We point out that in our model, for  $W > W_c$ , the com-

petition between attraction and repulsion has the effect to produce microphase structures, which are the analog of the cluster phase observed in colloidal system, characterized by a peak in the structure factor around a wave vector corresponding to the inverse of the typical size of the clusters. The width of the peak is related to the correlation length, which represents the range over which such modulated structures are locally ordered. In our model the modulated structures are the precursors of an equilibrium lamellar phase occurring at lower temperature. Therefore, according to this analogy, our results suggest that the cluster phase observed in colloidal suspensions might be the signature of the presence in the system phase diagram of an equilibrium lamellar phase, which is very often kinetically avoided on the experimental time scales. Such an underlying equilibrium ordered phase may strongly affect the dynamics of the system in the low temperature region, close to the colloidal gelation. The presence of a stripe/columnar/lamellar phase in the phase diagram and the emergence of microphase structures has been clearly shown in recent numerical simulations of model systems of particles interacting via the DLVO potential both in two [11, 12] and in three dimensions [14], where the presence of first order transitions from a cluster phase to periodically ordered phases has been clearly detected.

The nature of the glass transition found in our model gives many insights on the nature of the mechanisms inducing the phenomenon of colloidal gelation. We suggest that the structural arrest in colloidal suspensions might be due to the formation of microphase structures, which are ordered on small length scales, and are assembled together in a disordered fashion on larger length scales, thereby inducing a complex free energy landscape and, consequently, a complex and slow dynamics.

Notice that in our model there is no geometric frustration due to the hard-core excluded volume, which is totally absent in the Hamiltonian. The frustration lies only in the competition between attractive and repulsive interactions on different length scales. Therefore, our results seem to indicate that the physical mechanism inducing the structural arrest in charged colloids is totally different from that responsible for the jamming and the glass transition in molecular liquids at high volume fraction.

In real experiments the addition of salt increases the number of ions in the solution, thereby decreasing the strength of the repulsive shoulder of the potential. Our results suggest that there is a critical value of the ions concentration (corresponding to  $W_c$ ) above which no modulated structures are formed and the system undergoes, instead, a phase separation between a colloid-rich and a colloid-poor region.

All these prediction could be experimentally and numerically checked.

We warmly thank A. de Candia, E. Del Gado, A. Fierro, G. Gonnella and N. Sator. M.T. is grateful G.

Tarjus for many useful discussions and remarks. Work supported by EU Network Numbers HPRN-CT-2002-00307 and MRTN-CT-2003-504712, MIUR-PRIN 2004, MIUR-FIRB 2001, CRdC-AMRA, INFN-PCI.

### APPENDIX A: CRITICAL EXPONENTS OF THE FERROMAGNETIC TRANSITION IN THE HARTREE APPROXIMATION

In this appendix we compute the critical exponents of the second order ferromagnetic phase transition found within the Self-Consistent Hartree approximation for  $W < W_c$ .

As shown in Sec. III, for  $W < W_c$ , the correlation function,  $G(\mathbf{k})$ , has a maximum in  $|\mathbf{k}| = 0$ , where it equals  $T/(r + 4\pi W\lambda^2)$ . Therefore, as  $r \rightarrow r_c = -4\pi W\lambda^2$ , the susceptibility,  $\chi = G(|\mathbf{k}| = 0)/T$  diverges, corresponding to a second order critical point. Since the divergence occurs around  $|\mathbf{k}| = 0$ , in order to determine the critical behaviour, we can expand the Hamiltonian of Eq. (4) up to the lowest orders in  $k^2$ , as done in Eq. (17), neglecting the other irrelevant terms. According to Eq. (7), the susceptibility reads:

$$\chi^{-1}(r) = r + 4\pi W\lambda^2 = r - r_c \equiv \tau. \quad (\text{A1})$$

Replacing  $r$  and  $r_c$  with their expressions obtained via the self-consistent relation, Eq. (10), and expanding the correlators up to  $O(k^2)$ , we get:

$$\tau = \frac{3g}{2\pi^2} \int_0^\Lambda dk k^2 \left[ \frac{T}{r + 4\pi W\lambda^2 + (1 - 4\pi W\lambda^4)k^2} - \frac{T_c}{(1 - 4\pi W\lambda^4)k^2} \right]. \quad (\text{A2})$$

Now, we define the function  $I(\tau)$  as

$$I(\tau) = \int_0^\Lambda dk \frac{1}{\tau + ck^2}. \quad (\text{A3})$$

Recalling that  $\tau = r - r_c = r + 4\pi W\lambda^2 = 1 - W/W_c$  and that  $c = 1 - 4\pi W\lambda^4$  (note that  $c = 0$  for  $W = W_c$ ), in terms of the function  $I(\tau)$  Eq. (A2) can be written as:

$$\tau = \frac{3g(T - T_c)}{2\pi^2} \int_0^\Lambda dk \frac{ck^2}{\tau + ck^2} - \frac{3gT_c}{2\pi^2 c} \tau I(\tau). \quad (\text{A4})$$

The first integral appearing in the previous equation approaches a constant as  $\tau \rightarrow 0$ , whereas the integral  $I(\tau)$  is divergent as  $\tau \rightarrow 0$  as

$$I(\tau) \sim \tau^{-1/2}. \quad (\text{A5})$$

To the leading order in  $\tau$ , the left hand side of Eq. (A4) can be neglected, leading to

$$T - T_c \sim \tau^{1/2}, \quad (\text{A6})$$

and, thus:

$$\chi^{-1} = \tau^{-1} \sim (T - T_c)^{-2}. \quad (\text{A7})$$

This allows to determine the exponent  $\gamma$ :

$$\gamma = 2. \quad (\text{A8})$$

Within the self-consistent Hartree approximation, there are no  $\mathbf{k}$ -dependent corrections to the mean field propagator, all the corrections being included in the renormalized mass,  $r$ . Therefore,

$$\chi(\mathbf{k}) = [\tau + (1 - 4\pi W\lambda^4)k^2]^{-1} = \chi [1 + (k\xi)^2]^{-1}, \quad (\text{A9})$$

where

$$\xi^2 = (1 - 4\pi W\lambda^4)/\tau \sim (T - T_c)^{-2}. \quad (\text{A10})$$

This immediately leads to

$$\nu = \frac{\gamma}{2} = 1. \quad (\text{A11})$$

Similarly, it is possible to verify that also for  $W > W_c$ , at the spinodal line of the paramagnetic phase, located at  $T = 0$ , the susceptibility,  $\chi(k_m)$ , and the correlation length,  $\xi$ , diverge with the usual Hartree critical exponents.

### APPENDIX B: FLUCTUATION-INDUCED FIRST ORDER TRANSITION TO THE LAMELLAR PHASE

In this appendix we determine the first order transition temperature  $T_L(W, \lambda)$  from the homogeneous phase to the lamellar phase. We follow the approach taken in [27] for the Coulomb case and we generalize it to the case of a finite screening length of the repulsive potential. Let us introduce a spatially varying external field,  $h_{\mathbf{k}}$ , linearly coupled to the order parameter field  $\phi_{\mathbf{k}}$ . As a result,  $\phi_{\mathbf{k}}$  is now the sum of an average component,  $m_{\mathbf{k}} = \langle \phi_{\mathbf{k}} \rangle$ , and a fluctuation around it  $\xi_{\mathbf{k}} = \phi_{\mathbf{k}} - m_{\mathbf{k}}$ . The resulting equation of state for the average components reads [27]:

$$h_{\mathbf{k}} = \left( r_0 + k^2 + \frac{4\pi W}{\lambda^{-2} + k^2} \right) m_{\mathbf{k}} \quad (\text{B1})$$

$$+ g \int \frac{d^3 \mathbf{k}_1}{(2\pi)^3} \frac{d^3 \mathbf{k}_2}{(2\pi)^3} [m_{\mathbf{k}_1} m_{\mathbf{k}_2} + 3G(\mathbf{k}_1, \mathbf{k}_2)] m_{\mathbf{k} - \mathbf{k}_1 - \mathbf{k}_2},$$

where the connected correlation function  $G(\mathbf{k}, \mathbf{k}') = \langle \xi_{\mathbf{k}} \xi_{\mathbf{k}'} \rangle$ , is obtained self-consistently by solving

$$TG^{-1}(\mathbf{k}, \mathbf{k}') = \left( r_0 + k^2 + \frac{4\pi W}{\lambda^{-2} + k^2} \right) \delta(\mathbf{k} + \mathbf{k}') \quad (\text{B2})$$

$$+ 3g \int \frac{d^3 \mathbf{q}}{(2\pi)^3} [m_{\mathbf{q}} m_{\mathbf{k} + \mathbf{k}' - \mathbf{q}} + G(\mathbf{q}, \mathbf{k} + \mathbf{k}' - \mathbf{q})],$$

together with the unitarity condition:

$$\int \frac{d^3\mathbf{q}}{(2\pi)^3} G^{-1}(\mathbf{k}, \mathbf{q}) G(\mathbf{q}, \mathbf{k}') = \delta(\mathbf{k} - \mathbf{k}'). \quad (\text{B3})$$

Note that in the paramagnetic phase, when all  $h_{\mathbf{k}}$ , and  $m_{\mathbf{k}}$  are equal to zero, Eqs. (B1) and (B2) reduce to Eq. (10) with  $G(\mathbf{k}, \mathbf{k}') = G(\mathbf{k}) \delta(\mathbf{k} + \mathbf{k}')$ .

In the lamellar phase, characterized by the periodic order, instead, we consider:

$$h_{\mathbf{k}} = h(\delta(\mathbf{k} - \mathbf{k}_m) + \delta(\mathbf{k} + \mathbf{k}_m)), \quad (\text{B4})$$

and

$$m_{\mathbf{k}} = m(\delta(\mathbf{k} - \mathbf{k}_m) + \delta(\mathbf{k} + \mathbf{k}_m)), \quad (\text{B5})$$

where  $\mathbf{k}_m$  is given in Eq. (14). As shown by Brazovskii for a related model [34], in this region, the fluctuations of wave-vector  $\mathbf{k}$  with  $|\mathbf{k}| = k_m$  are dominant, and the effect of the off-diagonal terms with  $\mathbf{k} \neq \mathbf{k}'$  can be neglected in the correlation function. As a result,

$$TG^{-1}(\mathbf{k}) = r + k^2 + \frac{4\pi W}{\lambda^{-2} + k^2}. \quad (\text{B6})$$

This expression is formally equivalent to that of Eq. (10). However, in the case of a phase characterized by Eqs. (B4) and (B5) the renormalized mass,  $r$ , is given by:

$$\begin{aligned} r &= r_0 + 3g \int \frac{d^3\mathbf{k}}{(2\pi)^3} (G(\mathbf{k}) + |m_{\mathbf{k}}|^2) \\ &= r_0 + 3g \int \frac{d^3\mathbf{k}}{(2\pi)^3} \frac{T}{r + k^2 + \frac{4\pi W}{\lambda^{-2} + k^2}} + 6g|m|^2. \end{aligned} \quad (\text{B7})$$

By introducing Eqs. (B4)-(B7) in Eq. (B1) and recalling Eq. (14), one obtains the following equation of state:

$$\begin{aligned} h &= \left( r_0 + 2\sqrt{4\pi W} - \lambda^{-2} \right. \\ &\quad \left. + 3g \int \frac{d^3\mathbf{k}}{(2\pi)^3} \frac{T}{r + k^2 + \frac{4\pi W}{\lambda^{-2} + k^2}} + 3g|m|^2 \right) m \\ &= \left( r + 2\sqrt{4\pi W} - \lambda^{-2} - 3g|m|^2 \right) m. \end{aligned} \quad (\text{B8})$$

When we do not consider fluctuations ( $r \rightarrow r_0$ ), the last equation gives the mean field result.

Below some temperature, there is a coexistence of the paramagnetic phase and the lamellar phase. In zero field ( $h = 0$ ), the former is characterized by  $m = 0$  and the latter by  $m \neq 0$ , where  $m$  is solution of Eq. (B8), i.e.,  $(r + 2\sqrt{4\pi W} - \lambda^{-2} - 3g|m|^2) = 0$ . The transition point, which is then associated with a first order transition, is obtained as the temperature at which the free energies of the two phases are equal. It is convenient to calculate directly the free energy difference  $\Delta F(T)$  between the

lamellar ( $m \neq 0$ ) and the paramagnetic ( $m = 0$ ) phase at a given temperature  $T$  [27]:

$$\Delta F = \int_0^m dm' \frac{\partial F}{\partial m'} = 2 \int_0^m dm' h(m') \quad (\text{B9})$$

where  $h(m')$  is given by Eq. (B8). Changing the integration variable from  $m'$  to  $r'(m')$  solution of Eq. (B7), after some algebra we obtain:

$$\begin{aligned} g\Delta F &= \int_{r(m=0)}^{r(m)} dr' \left( \frac{r' + r_0}{2} + 2\sqrt{4\pi W} - \lambda^{-2} \right. \\ &\quad \left. + \frac{3gT}{4\pi^2} \int dk \frac{k^2}{r' + k^2 + \frac{4\pi W}{\lambda^{-2} + k^2}} \right) \\ &\quad \times \left( \frac{1}{6} + \frac{gT}{4\pi^2} \int dk \frac{k^2}{\left( r' + k^2 + \frac{4\pi W}{\lambda^{-2} + k^2} \right)^2} \right), \end{aligned} \quad (\text{B10})$$

where  $r(m=0)$  is the solution of Eq. (10) whereas  $r(m)$  and  $m$  are solutions of the following coupled equations:

$$\begin{cases} r + 2\sqrt{4\pi W} - \lambda^{-2} - 3g|m|^2 = 0 \\ r = r_0 + 3g \int \frac{d^3\mathbf{k}}{(2\pi)^3} \frac{T}{r + k^2 + \frac{4\pi W}{\lambda^{-2} + k^2}} + 6g|m|^2. \end{cases} \quad (\text{B11})$$

By solving Eqs. (B10) and (B11) numerically for several values of  $W$  and  $T$  (and for  $g = 1$ ,  $r_0 = -1$  and  $\lambda = 2$ ), we have found that, for any given value of  $W$ , the sign of  $\Delta F$  changes at a finite value of  $T = T_L$ , that marks the first order transition between paramagnetic and lamellar phases. The results are shown in Figs. 1 and 6. We also solved Eqs. (B9)-(B11) for several values of  $W$  and  $\lambda$  keeping the temperature  $T$  fixed. The transition line in the frustration ( $W$ )-range ( $\lambda$ ) plane is shown in the inset of Fig. 1.

### APPENDIX C: SELF-CONSISTENT SOLUTION FOR THE DYNAMICS IN THE SPHERICAL LIMIT

In this section we discuss the self-consistent solution of the dynamics of the model in the spherical approximation. More precisely, our aim is to solve self-consistently Eqs. (21) and (22). In order to do so we remember that:

$$\dot{Q}(t) = r + g \int \frac{d^3\mathbf{k}}{(2\pi)^3} G(\mathbf{k}, t). \quad (\text{C1})$$

From Eq. (21), we note that  $G(\mathbf{k}, t)$  has a maximum at a wave vector  $k_{max}(t)$  given by:

$$Q(t) = -2k_{max}^2(t)t - \frac{4\pi W \lambda^{-2} t}{(\lambda^{-2} + k_{max}^2(t))^2}, \quad (\text{C2})$$

which gives the expression of  $Q(t)$  in terms of the peak position  $k_{max}(t)$ . Inserting Eq. (C2) into Eq. (21) we

obtain that  $G(\mathbf{k}, t) = G(\mathbf{k}, 0) e^{-Mt f(k, t)}$ , where

$$f(k, t) = \frac{4\pi W k^2}{\lambda^{-2} + k^2} + k^4 - 2k^2 k_{max}^2(t) \quad (\text{C3})$$

$$- \frac{4\pi W \lambda^{-2} k^2}{(\lambda^{-2} + k_{max}^2(t))^2}.$$

Obviously,  $f(k, t)$  has a minimum for  $k = k_{max}(t)$ .

Now we can evaluate the integral in Eq. (C1) by means of the saddle point method, provided that  $Mt$  is large. This yields:

$$\dot{Q}(t) = r + B \frac{k_{max}^2(t)}{\sqrt{Mt f''(k_{max}, t)}} \quad (\text{C4})$$

$$\times \exp \left[ Mt \left( 1 - \frac{4\pi W}{(\lambda^{-2} + k_{max}^2(t))^2} \right) k_{max}^4(t) \right],$$

where  $B = 2g (\pi/2)^{3/2} G(k_{max}, 0)$ . Now, we can relate  $\dot{Q}(t)$  to  $k_{max}(t)$  through Eq. (C2) and, inserting the result in the previous equation, we obtain Eq. (23). The function  $P$  equals:

$$P = \frac{1}{B} \left[ -r - 2k_{max}^2(t) - \frac{4\pi W \lambda^{-2}}{(\lambda^{-2} + k_{max}^2(t))^2} - 4tk_{max}(t)F(k_{max}(t)) \frac{dk_{max}(t)}{dt} \right], \quad (\text{C5})$$

where  $F(k_{max}(t))$  is defined as:

$$F(k_{max}(t)) = \left( 1 - \frac{4\pi W \lambda^{-2}}{(\lambda^{-2} + k_{max}^2(t))^3} \right). \quad (\text{C6})$$

Inserting the right hand side of Eq. (23) into the expression of the time dependent structure factor we obtain:

$$G(\mathbf{k}, t) = G(\mathbf{k}, 0) \left[ \frac{P \sqrt{Mt F(k_{max}(t))}}{k_{max}(t)} \right] e^{-Mt \Delta f(k, t)}, \quad (\text{C7})$$

where  $\Delta f(k, t) = f(k, t) - f(k_{max}, t)$ . The position of the peak is given by the solution of Eq. (23). Taking the logarithm of both sides of Eq. (23) and dividing by  $Mt$  we obtain an asymptotic expression for  $k_{max}(t)$  which is readily analyzed in the limit  $t \rightarrow \infty$ .

$$\left( 1 - \frac{4\pi W}{(\lambda^{-2} + k_{max}^2(t))^2} \right) k_{max}^4(t) \quad (\text{C8})$$

$$= \frac{\ln \left[ -r - 2k_{max}^2(t) - \frac{4\pi W \lambda^{-2}}{(\lambda^{-2} + k_{max}^2(t))^2} \right]}{Mt}$$

$$+ \frac{1}{2} \frac{\ln [F(k_{max}(t))]}{Mt} - \frac{\ln [k_{max}(t)]}{Mt},$$

where we have neglected the terms which vanish in the asymptotic limit,  $t \rightarrow \infty$ . As explained in Sec. IV, depending on the values of  $W$  and  $\lambda$ , different solutions of the previous equation are found. In particular, one needs again to distinguish between the cases  $W < W_c$  and  $W > W_c$ .

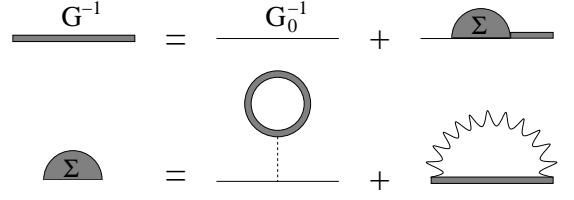


FIG. 7: Diagrams of the Self-Consistent Screening Approximation [17, 18, 25, 26].

#### APPENDIX D: SELF-CONSISTENT SCREENING APPROXIMATION

Here we discuss how to compute the complexity within the SCSA. This section is unessential, since all the calculations have been already extensively reported in the literature (see Ref. [26]). Nevertheless, we believe that this appendix might be useful for the sake of completeness.

Following Ref. [26], we first summarize a few properties of the matrices in the replica space with structure similar to Eq. (41). Introducing a matrix  $\mathbf{E}$  such that  $E_{ab} = 1$  and the unitary matrix  $\mathbf{1} = \delta_{ab}$ , it is easy to see that the product of any two  $m \times m$  matrices with structure:

$$\mathbf{A} = a_1 \mathbf{1} + a_2 \mathbf{E} \quad (\text{D1})$$

is given by:

$$\mathbf{A} \cdot \mathbf{B} = (a_1 b_1) \mathbf{1} + (a_1 b_2 + a_2 b_1 + m a_2 b_2) \mathbf{E}. \quad (\text{D2})$$

This relation leads to

$$\mathbf{A}^{-1} = \frac{1}{a_1} \mathbf{1} - \frac{a_2}{a_1 (a_1 + m a_2)} \mathbf{E} \quad (\text{D3})$$

for the inverse of a matrix  $\mathbf{A}$ . These properties will be used in the following.

In the SCSA, the self-energy,  $\Sigma_{ab}$  is given by (see Fig. 7):

$$\Sigma_{ab}(\mathbf{k}) = \frac{2}{N} \int \frac{d^3 \mathbf{q}}{(2\pi)^3} G_{ab}(\mathbf{k} + \mathbf{q}) D_{ab}(\mathbf{q}), \quad (\text{D4})$$

where

$$D_{ab}(\mathbf{q}) = \left[ (gT)^{-1} + \Pi_{ab}(\mathbf{q}) \right]^{-1} \quad (\text{D5})$$

is determined self-consistently by the polarization function

$$\Pi_{ab}(\mathbf{q}) = \int \frac{d^3 \mathbf{p}}{(2\pi)^3} G_{ab}(\mathbf{q} + \mathbf{p}) G_{ba}(\mathbf{p}). \quad (\text{D6})$$

The ansatz Eq. (41) for the correlation functions implies an analogous structure for  $\Sigma_{ab}(\mathbf{k})$  and  $\Pi_{ab}(\mathbf{k})$ . Inserting this ansatz into  $\Pi_{ab}(\mathbf{q})$  gives:

$$\Pi(\mathbf{q}) = [\Pi_G(\mathbf{q}) - \Pi_{\mathcal{F}}(\mathbf{q})] \mathbf{1} + \Pi_{\mathcal{F}}(\mathbf{q}) \mathbf{E}. \quad (\text{D7})$$

where the diagonal and off-diagonal elements of the polarization function are:

$$\Pi_{\mathcal{G}}(\mathbf{q}) = \int \frac{d^3\mathbf{p}}{(2\pi)^3} \mathcal{G}(\mathbf{q} + \mathbf{p}) \mathcal{G}(\mathbf{p}), \quad (\text{D8})$$

$$\Pi_{\mathcal{F}}(\mathbf{q}) = \int \frac{d^3\mathbf{p}}{(2\pi)^3} \mathcal{F}(\mathbf{q} + \mathbf{p}) \mathcal{F}(\mathbf{p}).$$

Using the property expressed in Eq. (D2), it is now straightforward to determine  $D_{ab}(\mathbf{q})$  which, in the limit  $m \rightarrow 1$ , is given by:

$$D_{\mathcal{G}}(\mathbf{q}) = [\mathcal{D}_{\mathcal{G}}(\mathbf{q}) - \mathcal{D}_{\mathcal{F}}(\mathbf{q})] \mathbf{1} + \mathcal{D}_{\mathcal{F}}(\mathbf{q}) \mathbf{E}, \quad (\text{D9})$$

where

$$\mathcal{D}_{\mathcal{G}}(\mathbf{q}) = \left[ (gT)^{-1} + \Pi_{\mathcal{G}}(\mathbf{q}) \right]^{-1}, \quad (\text{D10})$$

$$\mathcal{D}_{\mathcal{F}}(\mathbf{q}) = - \frac{\Pi_{\mathcal{F}}(\mathbf{q}) \mathcal{D}_{\mathcal{G}}^2(\mathbf{q})}{1 - \Pi_{\mathcal{F}}(\mathbf{q}) \mathcal{D}_{\mathcal{G}}(\mathbf{q})}.$$

Analogously, inserting the above equation into Eq. (D4), we get for the self-energies

$$\Sigma(\mathbf{q}) = [\Sigma_{\mathcal{G}}(\mathbf{q}) - \Sigma_{\mathcal{F}}(\mathbf{q})] \mathbf{1} + \Sigma_{\mathcal{F}}(\mathbf{q}) \mathbf{E}, \quad (\text{D11})$$

where

$$\Sigma_{\mathcal{G}}(\mathbf{q}) = \frac{2}{N} \int \frac{d^3\mathbf{p}}{(2\pi)^3} \mathcal{D}_{\mathcal{G}}(\mathbf{p}) \mathcal{G}(\mathbf{q} + \mathbf{p}), \quad (\text{D12})$$

$$\Sigma_{\mathcal{F}}(\mathbf{q}) = \frac{2}{N} \int \frac{d^3\mathbf{p}}{(2\pi)^3} \mathcal{D}_{\mathcal{F}}(\mathbf{p}) \mathcal{F}(\mathbf{q} + \mathbf{p}). \quad (\text{D13})$$

This set of equations is closed by the Dyson Equation, Eq. (40):

$$G_{ab}^{-1}(\mathbf{k}) = [G_0(\mathbf{k}) + \Sigma_{\mathcal{G}}(\mathbf{k}) - \Sigma_{\mathcal{F}}(\mathbf{k})] \delta_{ab} + \Sigma_{\mathcal{F}}(\mathbf{k}), \quad (\text{D14})$$

which, in the limit  $m \rightarrow 1$ , according to Eq. (D3), gives:

$$\mathcal{G}^{-1}(\mathbf{k}) = G_0^{-1}(\mathbf{k}) + \Sigma_{\mathcal{G}}(\mathbf{k}) \quad (\text{D15})$$

for the diagonal elements, and

$$\begin{aligned} \mathcal{F}(\mathbf{k}) &= - \frac{\mathcal{G}^2(\mathbf{k}) \Sigma_{\mathcal{F}}(\mathbf{k})}{1 - \mathcal{G}(\mathbf{k}) \Sigma_{\mathcal{F}}(\mathbf{k})} \\ &= \mathcal{G}(\mathbf{k}) - \frac{1}{\mathcal{G}^{-1}(\mathbf{k}) - \Sigma_{\mathcal{F}}(\mathbf{k})}, \end{aligned} \quad (\text{D16})$$

for the off-diagonal ones.

Within the self-consistent screening approximation, the free energy assumes the following expression [18, 19, 25, 26]:

$$\frac{F(m)}{2mT} = \text{Tr} \ln G^{-1} + \text{Tr} \ln D^{-1} + \text{Tr} G \Sigma. \quad (\text{D17})$$

The evaluation of the traces in the replica space is straightforward. After that we are able to perform the derivative with respect to the number of replicas in order to compute the complexity,  $\Sigma$ , according to Eq. (38). To this aim we have to take the analytical continuation to  $m \rightarrow 1$ . The configurational entropy can be written as the sum of two contributions [25, 26]:

$$\Sigma = \Sigma^{(1)} + \Sigma^{(2)}, \quad (\text{D18})$$

where

$$\Sigma^{(1)} = \frac{1}{2} \int \frac{d^3\mathbf{k}}{(2\pi)^3} \left\{ \ln \left( 1 - \frac{\mathcal{F}(\mathbf{k})}{\mathcal{G}(\mathbf{k})} \right) + \frac{\mathcal{F}(\mathbf{k})}{\mathcal{G}(\mathbf{k})} \right\}, \quad (\text{D19})$$

and

$$\begin{aligned} \Sigma^{(2)} &= \frac{1}{2} \int \frac{d^3\mathbf{k}}{(2\pi)^3} \left\{ \ln \left( 1 - \frac{gT \Pi_{\mathcal{F}}(\mathbf{k})}{1 + gT \Pi_{\mathcal{G}}(\mathbf{k})} \right) \right. \\ &\quad \left. + \frac{gT \Pi_{\mathcal{F}}(\mathbf{k})}{1 + gT \Pi_{\mathcal{G}}(\mathbf{k})} \right\}. \end{aligned} \quad (\text{D20})$$

From Eqs. (D19-D20) and Eq. (D16), it immediately follows that  $\Sigma = 0$  if  $\mathcal{F}(\mathbf{k})$  vanishes or, equivalently, if  $\Sigma_{\mathcal{F}}(\mathbf{k})$  vanishes.

Solving numerically Eqs. (D8)-(D16) we get the expressions of the correlators,  $\mathcal{G}(\mathbf{k})$  and  $\mathcal{F}(\mathbf{k})$ , of the self-energies,  $\Sigma_{\mathcal{G}}(\mathbf{k})$  and  $\Sigma_{\mathcal{F}}(\mathbf{k})$ , and of the polarization functions,  $\Pi_{\mathcal{G}}(\mathbf{k})$  and  $\Pi_{\mathcal{F}}(\mathbf{k})$ . Then, according to Eqs. (D19) and (D20) we are able to compute the complexity,  $\Sigma$ .

- 
- [1] W.B. Russel, D.A. Saville, and W.R. Schowalter, *Colloidal Dispersions* (Cambridge University Press, Cambridge, U.K., 1989); I.D. Morrison and S. Ross *Colloidal Dispersions: Suspensions, Emulsions and Foams* (Wiley-Interscience, New York, 2002).
- [2] W. van Meegen, S.M. Underwood and P.N. Pusey, Phys. Rev. Lett. **67**, 1586 (1991).
- [3] V.J. Anderson and H.N.W. Lekkerkerker, Nature **416**,

811 (2002).

- [4] A. Stradner, H. Sedgwick, F. Cardinaux, W.C.K. Poon, S.U. Egelhaaf, and P. Schurtenberger, Nature **432**, 492 (2004).
- [5] A.I. Campbell, V. J. Anderson, J. S. van Duijneveldt and P. Bartlett, Phys. Rev. Lett. **94**, 208301 (2005).
- [6] J.N. Israelachvili, *Intermolecular and surface forces*, (Academic press, London, 1985); J.C. Crocker and D.G.



- Grier, Phys. Rev. Lett. **73**, 352 (1994).
- [7] P.N. Segre, V. Prasad, A.B. Schofield, and D.A. Weitz, Phys. Rev. Lett. **86**, 6042 (2001).
- [8] F. Sciortino, S. Mossa, E. Zaccarelli and P. Tartaglia, Phys. Rev. Lett. **93**, 055701 (2004).
- [9] S. Mossa, F. Sciortino, P. Tartaglia, and E. Zaccarelli, Langmuir **20**, 10756 (2004); F. Sciortino, P. Tartaglia and E. Zaccarelli, J. Phys. Chem. B **109**, 21942 (2005).
- [10] A. Coniglio, E. Del Gado, A. Fierro, A. Coniglio, J. Phys.: Condens. Matter **16**, S4831 (2004); A. de Candia A, E. Del Gado, A. Fierro, N. Sator, A. Coniglio, Physica A **358**, 239 (2005).
- [11] P. Charbonneau and D.R. Reichman, cond-mat/0604430.
- [12] A. Imperio and L. Reatto, J. Phys.: Condens. Matter **16**, S3769 (2004).
- [13] M. Tarzia and A. Coniglio, Phys. Rev. Lett. **96**, 075702 (2006).
- [14] A. de Candia, E. Del Gado, A. Fierro, N. Sator, M. Tarzia, and A. Coniglio, Phys. Rev. E **74**, 010403(R) (2006).
- [15] The model can be thought as the continuum limit of a lattice gas model described by the following Hamiltonian:  $\mathcal{H} = -\epsilon \sum_{\langle ij \rangle} n_i n_j + W \sum_{i \neq j} \frac{e^{-|i-j|/\lambda}}{|i-j|} n_i n_j + \mu \sum_i n_i$ , where  $n_i = 1, 0$  whether the site  $i$  is occupied by a particle or not. In this paper we only consider the values of the chemical potential  $\mu$  for which  $\langle n_i \rangle = 0.5$ .
- [16] R. Monasson, Phys. Rev. Lett. **75**, 2847 (1995).
- [17] M. Mézard and G. Parisi, Phys. Rev. Lett. **82**, 747 (1999).
- [18] A.J. Bray, Phys. Rev. Lett. **32**, 1413 (1974).
- [19] M. Mézard and A.P. Young, Europhys. Lett. **18**, 653 (1992).
- [20] S.W. Wu, H. Westfahl, J. Schmalian, P.G. Wolynes, Chem. Phys. Lett. **359**, 1 (2002).
- [21] V.J. Emery and S.A. Kivelson, Physica C **209**, 597 (1993); U. Löw, V.J. Emery, K. Fabricius and S.A. Kivelson, Phys. Rev. Lett. **72**, 1918 (1994).
- [22] S.C. Glotzer and A. Coniglio, Phys. Rev. E **50**, 4241 (1994).
- [23] Z. Nussinov, J. Rudnick, S. A. Kivelson and L. N. Chayes, Phys. Rev. Lett **83**, 472 (1999).
- [24] D. Kivelson, S. A. Kivelson, X. L. Zhao, Z. Nussinov, and G. Tarjus, Physica A **219**, 27 (1995); P. Viot, P. Viot, G. Tarjus and D. Kivelson, J. Chem. Phys. **112**, 10368 (2000).
- [25] J. Schmalian and P.G. Wolynes, Phys. Rev. Lett. **85**, 836 (2000).
- [26] H. Westfahl, J. Schmalian and P.G. Wolynes, Phys. Rev. B **64**, 174203 (2001).
- [27] M. Grousson, V. Krakoviack, G. Tarjus and P. Viot, Phys. Rev. E **66**, 026126 (2002).
- [28] M. Seul and D. Andelman, Science **267**, 476 (1995); C.M. Knobler and R.C. Desai, Annu. Rev. Phys. Chem. **43**, 207 (1992).
- [29] C. Roland and R.C. Desai, Phys. Rev. B **42**, 6658 (1990); L.Q. Chen and A.G. Khachatryan, Phys. Rev. Lett. **70**, 1477 (1993); C. Sagui and R.C. Desai, *ibid.* **71**, 3995 (1993); A.J. Dickstein, S. Erramilli, R.E. Goldstein, D.P. Jackson, and S.A. Langer, Science **261**, 1012 (1993);
- [30] T. Ohta and K. Kawazaki, Macromolecules **19**, 2621 (1986); L. Leibler, Macromolecules **13**, 1602 (1980).
- [31] F.H. Stillinger, J. Chem. Phys. **78**, 4654 (1983); H.J. Woo, C. Carraro and D. Chandler, Phys. Rev. E **52**, 6497 (1995).
- [32] J.M. Tranquada, B.J. Sternlieb, J.D. Axe, Y. Nakamura, S. Uchida, Nature **375**, 561 (1995).
- [33] P.M. Chaikin and T.C. Lubensky, *Principles of condensed matter physics*, (Cambridge Univ. Press, 1995).
- [34] S.A. Brazovskii, Z. Eksp. Teor. Fiz. **68**, 175 (1975) [Sov. Phys. JETP **41**, 85 (1975)]; G.H. Fredrickson and E. Helfand, J. Chem. Phys. **87**, 697 (1987).
- [35] J.W. Cahn and J.E. Hilliard, J. Chem. Phys. **28**, 258 (1958); A.J. Bray, Adv. Phys. **43**, 357 (1994).
- [36] S.C. Glotzer and A. Coniglio, Phys. Rev. E **50**, 4241 (1994); A. Coniglio and M. Zannetti, Europhys. Lett. **10**, 575 (1989); A. Coniglio, P. Ruggiero, and M. Zannetti, Phys. Rev. E **50**, 1046 (1994).
- [37] J. H. Cho, F. Borsa, D. C. Johnston and D. R. Torgeson, Phys. Rev. B **46**, R3179 (1992); S. H. Lee and S. W. Cheong, Phys. Rev. Lett. **79**, 2514 (1997); J. M. Tranquada, N. Ichikawa and S. Uchida, Phys. Rev. B **59**, 14712 (1999); M.-H. Julien, F. Borsa, P. Carretta, M. Horvatić, C. Berthier, and C.T. Lin, Phys. Rev. Lett. **83**, 604 (1999).
- [38] M. Grousson, G. Tarjus and P. Viot, Phys. Rev. Lett. **86**, 3455 (2001).
- [39] F. Corberi, G. Gonnella, and A. Lamura, Phys. Rev E **66** 016114 (2002); A.G. Xu, G. Gonnella, A. Lamura A, G. Amati, and F. Massaioli, Europhys. Lett. **71**, 651 (2005).
- [40] This issue has been also investigated in P.L. Geissler and D.R. Reichman, Phys. Rev. E **69**, 021501 (2004).
- [41] The applicability of the SCSA is supported by the fact that the large  $N$  limit is not singular.
- [42] Z. Nussinov, cond-mat/0506554.